Impact of instantaneous curvature on force and heat generation in manufacturing processes – a mathematical modelling

Sreerag C., Gokul R., Vinaykumar J. and Rajyalakshmi G.
Vellore Institute of Technology, Vellore, India

Received 28 June 2019
Revised 3 November 2019
27 December 2019
17 January 2020
Accepted 20 January 2020

Abstract

Purpose – In any machining process, the surface profile of the workpiece is continuously changing with respect to time and input parameters. In a conventional machining process, input parameters are feed and depth of cut whilst other parameters are considered to be constant throughout the process.

Design/methodology/approach – The direct and indirect participation of this instantaneous curvature can be used to optimize the strategy of cutting operation in terms of different parameters like heat generation-induced stresses, etc. The concepts of the metric tensor and Riemannian curvature tensor are made use in this study as a representation of curvature itself. The objective of this study is to create a mathematical methodology that can be implemented on a highly flexible machining process to find an optimum cutting strategy for a particular output parameter.

Findings – The study also includes different case studies for the validation of this newly introduced mathematical methodology.

Originality/value – The study will also find its position in other mechanical processes like forging and casting where instantaneous curvature affects various mechanical properties.

Keywords Machining process, Metric tensor, Riemannian tensor, Forging, Instantaneous curvature

Paper type Research paper

Nomenclature

x^p = Resultant tool direction;
x^n = n^{th} coordinates of the surface;
R^d_{ijk} = Riemann curvature tensor;
g_{ij} = Metric tensor;
X = Maximum tool path covered;
R = Radius of the cylindrical specimen in the turning operation;
Φ = Tool inclination angle;
t = Instantaneous time;
H^T = Component of heat absorbed by the tool;
H^C = Component of heat absorbed by the chip;
μ = Coefficient of friction;
H^P = Total heat energy;
F_c = Cutting force;
β = Friction angle;
α = Rake angle;
V = Velocity of the cutting tool on resultant path x^p;
x^t = Tangential direction of x^p;

Engineering Computations
Vol. 37 No. 7, 2020
pp. 2251-2273

0264-4401
DOI 10.1108/EC-06-2019-0289

x^c = Cutting force direction of x^p;
$H^{W/P}$ = Component of heat absorbed by the specimen; and
E = Component of heat transferred to surroundings.

1. Introduction

As we are aware, different mechanical parameters like heat generation (including heat generated on workpiece, tool and chip), stresses and so on are found to be directly related to the cutting strategy. Cutting strategy is the term describing the path of the material removal to form a final product in credit. In the near future, highly flexible machining operations with multi-dimensional cutting operation carried out in the same instant of time and optimal cutting stategy are to be customized accordingly for different output parameters, using a curvature-based methodology. The optimization of cutting stategy is found to be a resonable argument to obtain a quality product in any subtractive manufacturing process. The study particularly focuses on dynamical strain associated with forging and the estimation of heat generation (in terms of dynamic surface curvatures) during any machining process along with cutting parameters, tool geometry, work piece properties and tool path. This helps us to determin the ideal tool path during machining with minimum heat generation. The application of mathematical tools, including Riemann and metric tensors, as the representation of the curvature, is used to know how the curvature is instantaneously varying with respect to time and a function of cutting parameters like feed rate, depth of cut, spindle speed, which affect the mechanical behaviour of machined work piece in terms of stresses, heat generation, are made use of. With the help of metric tensors, the variation in the instantaneous geodesic relationship is also taken into account as a function of different parameters discussed above.

The heat generation and deployment of this generated heat are equally critical. The cutting strategy can be used to identify which path or cutting philosophy is more feseable to reduce heat generation. However, cutting without heat generation is an entirely impossible thing. Hence, in what proportion the heat is deployed in the tool, work piece, chip and to the environment should be addressed adequately.

1.1 Manufacturing background

Ay and Yang (1998) conducted experiments to predict the maximum heat generated in a machining process. They used an infrared camera and thermocouples for temperature measurement. They also derived a mathematical model to determine the temperature on tool surface during machining. Ostafiev *et al.* (1999) put forward a procedure to determine the tool temperature during the machining process, and later, it is validated with experimental results. Lazoglu and Altintas (2002) studied the temperature distribution during continuous and interrupted cutting. A steady-state model is used to predict the continuous cutting process, and a transient model is used for interrupted cutting process. The proposed model is used for calculating the tool geometry, cutting feed and depth of cut for minimum heat generation. Subbiah and Melkote (2008) studied the effect of cutting speed, depth of cut and rake angle in an orthogonal machining process. The study also includes how chip formation and cutting forces vary with respect to the selected parameters. Abukhshim *et al.* (2006) studied the temperature distribution in the tool during a turning process. They studied the heat generated in the rake surface of the tool due to the chip tool interaction, which significantly affects the tool life. Their prediction holds well in the linear region of the metal. Uzorh Augustine and Nwufo Olisaemeka (2013) used the inverse heat conduction formula to obtain a mathematical model for the heat generated in the tool chip interface. Heat generated due to the movement of chip over the rake surface and total shear energy are considered.

Denkena *et al.* (2016) studied heat generation in a thin work piece during a milling operation. Thin work pieces lose their stiffness due to the heat generated during machining, which makes this study more relevant. As an outcome of this study, it is suggested to use tools with a chamfered cutting edge rather than a sharp cutting edge, which can improve the work piece stability. Attia *et al.* (2016) presented a method to determine convective coefficient of heat transfer, which is essential for the calculation of heat generation. Kondratiev's regular regime theory is used to tobtain a relation between convective coefficient and process variables.

Ribeiro *et al.* (2018) studied about the heat generated in the work piece during a micro-milling process. He used the Greens theorem along with the Fourier transform for the mathematical modelling of the system. Abhang and Hameedullah (2010) derived a second-order mathematical model for the heat generated during a turning process using response surface methodology. The cutting parameters discussed in the study were cutting speed, depth of cut, feed and nose radius. Carvalho *et al.* (2006) derived a mathematical model to obtain the transient heat flux and temperature distribution in the cutting tool. The study exhibited the heat flux, which was considered as a constant varying with respect to time. Putz *et al.* (2016) studied the heat generated in a milling operation and derived a numerical model for the same. This model is useful to calculate the heat generated in continuous and interrupted cutting. Onyechi *et al.* (2013) derived a finite element model to obtain the stress and temperature distribution on the rake surface of the tool. The study reflected the effect of cutting temperature on the tool life and tool wear. Sun *et al.* (2017) discussed heat generation during milling of the Ti6Al4V alloy and highlighted on developing a mathematical model for the heat generated and its validation through experimentally measuring the tool workpiece temperature using a semi-artificial thermocouple. Klocke *et al.* (2015) studied the temperature fields in a machining process. The model used is derived on the basis of potential theory. The model used material properties along with the machining parameters.

Melzi *et al.* (2017) focused on the heat generation in a high-speed turning operation. They derived a mathematical model and used it to determine the optimum cutting parameters. They observed an increase in the cutting temperature on account of increase in cutting speed and feed. Pervaiz *et al.* (2014) combined computational fluid dynamics (CFD) and finite element analysis (FEA) to predict the temperature in the tool tip while machining. DEFORM 2D and ANSYS CFX were the software tools used for the simulation. They further studied the heat generation during flooded lubrication and minimum quantity lubrication cases. Li and Liang (2006) developed a mathematical model for near-dry machining application. They validated their model by machining medium carbon steel with uncoated carbide cutting tools. They noticed the cutting speed as a significant factor for the heat generation. Patru *et al.* (2019) machined aluminium 6015 alloy and observed the corresponding heat generated in the tool work piece interface. Using the response surface methodology, they developed a mathematical model to predict the cutting temperature based on the speed, feed and depth of cut as an input parameters. Fata *et al.* (2012) concentrated on the heat generation in a cutting tool during a turning operation. Here, C45 was used as the material and carbide cutting tool inserts for the machining purpose. FEM calculations facilitated obtaining the three-dimensional (3D) temperature field on the tool. In a general machining process, 99 per cent of the work done is shared as heat accumulated on the chip, tool and work piece, and the remaining 1 per cent is found stored as an elastic or other energy form. Out of the entire heat generated, 80 per cent is carried by the chip, 10 per cent by the tool and the balance 10 per cent contributes to the rise in the work piece temperature (Kumar *et al.*, 2015). In micromachining processes like micro-turning, micro-milling, majority of the heat is transferred to the chip and the same can be fairly approximated as 75 per cent and the

remaining 7 and 18 per cent correspond to the heat generation on the tool in operation and the work piece, repectively. However, in operations like micro-grinding and honing, the majority of the heat is transferred to the work piece alone.

1.2 Mathematical background

The concept of tensors has been already applied to explain many scientific phenomena in the history of modern science. This ranges from the very understanding of how far two continents are spaced in between and realising the complex four-dimensional (4D) space-time continuem mathematically. There are a variety of tensors like Riemann curvature tensor, metric tensor, Ricci tensor and so on. Ricci tensor is nothing but the 3D or volumentic curvature tensor that is an extra-dimensional form of the Riemann curvature tensor itself. The fundamental relation between the metric tensor and the curvature tensor is well established in many literatures. Article (McIntosh and Halford, 1981) is one of the studies focused on identifying the metric tensor from the Riemann curvature tensor. The fundamentals of the metric tensors can be referred from many literature sources. Article (Borisenko and Tarapov, 1979) is a motivational article concentrated on the the application relating to the metric tensor, which also excovers the wide possibilities of the application of the metric tensor in physical envionments. The geometrical meaning and the feasibilities of these mathematical terminologies are very important to develop and assign various applications related to pure mechanical manufacturing engineering and machining situations. Some articles (O'Neill, 2006; Dodson and Poston, 2013) noticed serve this purpose exclusively. There are some conferred works (Narain *et al.*, 2013) provoding geometrical philosophy as well as the algebra behind the metric tensor.

Though there are numerous studies on the effect of various machining parameters like heat generation, residual sress and so on, the importance of curvature change or the rate of change in curvature is not well addressed yet in such studies. Major results we are using in the manufacturing operations in the current literature are more machine-based, the knowledge about the impact of curvature in the manufacturing process will pave the way for highly flexible manufacturing techniques. In the flexible manufacturing process, machines are independent of a constrained path of operation, and hence enable machining through multiple paths or even on a entire surface. The knowledge about the influence of curvature will likewise help to optimise machining stategies to reduce the undesirable effects like heat generation to a great extent in a flexible manufacturing poit of view. In addition to subtractive manufacturing, the latest innovations like layer-by-layer additive manufacturing, construction of 4D printing using shape memmory polymers and so on also demand further urge of curvature-based studies in the manufacturing sector. The very fundamental ideas related to sufaces curvature effects can be used to build up a useful mathematical methodology in the manufacturing engineering sector to tackle the current dilemma relating to the heat generation and other outputs. Hence, the speed and flexibility of manufacturing philosophy deserve adequate curvature analysis and further studies.

2. Mathematical modelling

The mathematical modelling of the problem requires some assumptions. One of the major assumptions is the metric tensor/Riemann curvature tensor as a function of time or time coordinate, because the surface coordinates are instantaneously varying and should be a function of the resultant tool speed and tool path, which are the input parameters. The final assumption is that the resultant tool speed and material removal are in the same direction x^p. Figure 1 represents the transformation of cylindrical surface coordinates (x^1, x^2) in to a new coordinates (x^3, x^4) for better understanding of the mathematical concepts used.

Figure 1.
Transformation of coordinates

2.1 Riemann curvature tensor modelling or curvature modelling

A closed loop for elementary surface, as shown in Figure 2, is taken here. On integrating the angular difference obtained through parallel transport theorem provides the Riemann curvature tensor.

The amount of curvature depends on relative tool path and relative velocity of cutting tool.

Hence, using the Riemann curvature tensor:

$$R^{d}_{ijk} = f\left(\frac{dx^{p}}{dt}, x^{p}\right) \tag{2.1}$$

where:

R^{d}_{ijk}, is the measure of curvature known as curvature tensor, where (j,k) are surface coordinates, $d$and $i$are the direction of the initial and the instantaneous resultant vectors, respectively.

$\frac{dx^{p}}{dt}$ is the velocity of the cutting tool.

Let us assume:

$$R^{d}_{ijk} = A\left(\frac{dx^{p}}{dt}\right)^{n} + B(x^{p})^{m} + \phi \tag{2.2}$$

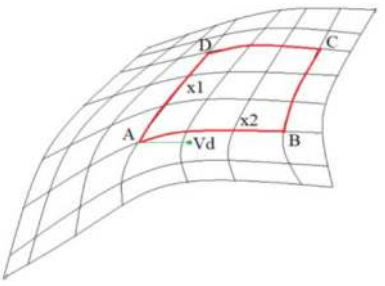

Figure 2.
Elementary representation of curvature

where A, B, ϕ are constants and $n = m = 1$ with the following boundary conditions:

$$R^d_{ijk}(t = 0) = R^d_{a12} \tag{2.3}$$

$$R^d_{ijk}(t = T) = R^d_{a34} \tag{2.4}$$

and x^p is the direction of the resultant tool path.

On applying boundary conditions in (2.2):

$\phi = R^d_{a12}$, and

$$AV + BX = R^d_{a34} - R^d_{a12} \quad \text{where,} \quad \left(\frac{dx^p}{dt}\right) = V, (x^p) = X$$

Equation (2.2) becomes:

$$R^d_{ijk} = A\left(\frac{dx^p}{dt}\right)^n + B(x^p)^m + R^d_{a12} \tag{2.5}$$

Comparing this solution with Riemann–Cristoffel curvature tensor:

$$R^d_{ijk} = \Gamma^d_{ik,j} - \Gamma^d_{ij,k} + \Gamma^\mu_{ik}\Gamma^d_{j\mu} - \Gamma^\mu_{ij}\Gamma^d_{k\mu} \tag{2.6}$$

We get the relation:

$$\Gamma^d_{ik,j} - \Gamma^d_{ij,k} + \Gamma^\mu_{ik}\Gamma^d_{j\mu} - \Gamma^\mu_{ij}\Gamma^d_{k\mu} = A\left(\frac{dx^p}{dt}\right)^n + B(x^p)^m + R^d_{a12} = R^d_{ijk} \tag{2.7}$$

The solving of equation (2.7) is comparatively difficult. Hence, instead of Riemann curvature tensors, we are using relative metric tensors to reduce the complexity and to include the same curvature with different magnification.

2.2 Metric tensor modelling or coordinate transfer modelling

2.2.1 Concept of geodesic and metric tensor. Geodesic is the shortest distance between two points on a surface. The difference in the metric tensor of two different surface geometries, flat surface Figure 3 and curved surface Figure 4, are discussed below separately.

Flat surface

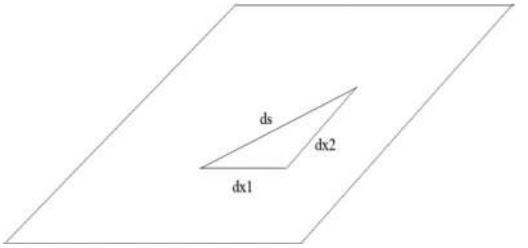

Figure 3.
Flat surface

Here, we can use Pythagorean theorem directly:

$$(ds)^2 = (dx^1)^2 + (dx^2)^2$$

$$(ds)^2 = \Sigma g_{ij} dx^1 . dx^2$$

where, metric tensor g_{ij}:

$$g_{ij} = \begin{pmatrix} 1 & 0 \\ 0 & 1 \end{pmatrix}$$

Curved surface:

Here, $g_{ij} = \begin{pmatrix} g_{11} & g_{12} \\ g_{21} & g_{22} \end{pmatrix}$

The metric modelling is similar to the Riemann modelling discussed above.

In this case, equation (2.5), thus, becomes:

$$g_{ij} = A_1 \left(\frac{dx^p}{dt}\right)^n + B_1 (x^p)^m + g_{12} \tag{2.8}$$

3. Case study I – uniform compression

Consider a flat surfaced work piece with a manufacturing process as uniform compression with constant load as shown in Figures 5(a)-(b):

As there is no change in curvature:

$$\frac{\partial R^d_{ijk}}{\partial t} = R^d_{ijk,t} = 0 \tag{3.1}$$

On differentiating equation (2.5) with respect to time:

$$\frac{\partial R^d_{ijk}}{\partial t} = R^d_{ijk,t} = A\left(\frac{d^2 x^p}{dt^2}\right) + B\left(\frac{dx^p}{dt}\right) = 0 \tag{3.2}$$

Hence, in this case:

$$A\left(\frac{d^2 x^p}{dt^2}\right) + B\left(\frac{dx^p}{dt}\right) = 0$$

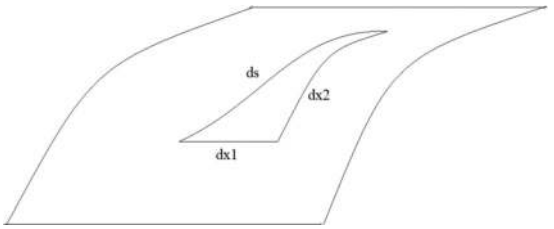

Figure 4.
Curved surface

$$\left(\frac{d^2x^p}{dt^2}\right) + BA^{-1}\left(\frac{dx^p}{dt}\right) = 0$$

$$(D^2 + BA^{-1}D)x^p = 0 \quad D = 0, D = -BA^{-1}$$

As RHS is zero, the complementary function (CF) will be the solution. Therefore,

$$x^p = c_1 e^{BA^{-1}} + c_2$$

With boundary conditions:

$$x^p(t = 0) = 0, x^p(t = T) = X$$

where X is the maximum tool path covered (maximum distance covered by the punch).

On solving equation (3.2):

$$c_1 = X\left(e^{-BA^{-1}T} - 1\right)^{-1}$$

$$c_2 = -X\left(e^{-BA^{-1}T} - 1\right)^{-1}$$

Hence, the solution for instantaneous strain is:

$$\frac{x^p}{X} = 1 - e^{-BA^{-1}(T+t)} - e^{-BA^{-1}t} + e^{-BA^{-1}T} \tag{3.3}$$

The effect of the BA^{-1} ratio in the instantaneous strain is analysed and the expectation curve based on various BA^{-1} discussed in Figure 6 as shown below.

The analysis is done in ANSYS and model creation in dynamic structural package.

The BA^{-1} is found to be proportional to the force applied.

Note: The BA^{-1} ratio is the shape-determining factor in the strain–time curve. In the case of hot forging and casting, BA^{-1} may also be a function of force, temperature and material properties. $BA^{-1} \gg 1$ is more feasible to explain gaseous materials and $BA^{-1} \ll 1$ for solid

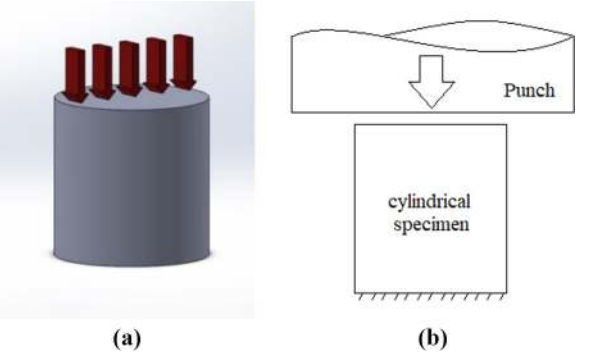

Figure 5.
(a-b) (a) represents deployment of compressive forces (b) represents pictorial diagram for uniform compression

materials. The analysis and comparison graph (numerical and mathematical modelling) are provided in Figures 7 and 8, respectively, for validation.

The deviation in between the mathematical and numerical value observed as the error notified in the Table I given below, where error value is the difference between mathematical and numerical results.

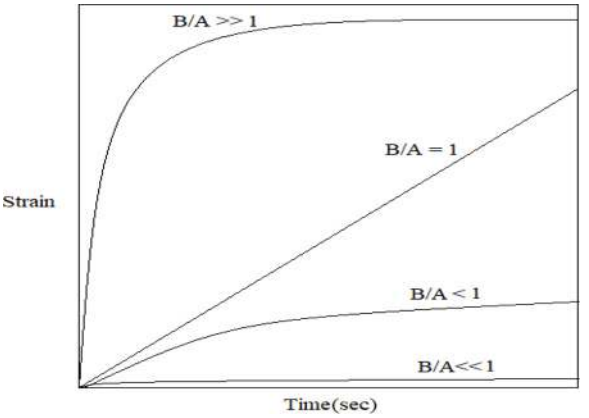

Figure 6.
BA^{-1} Plotting

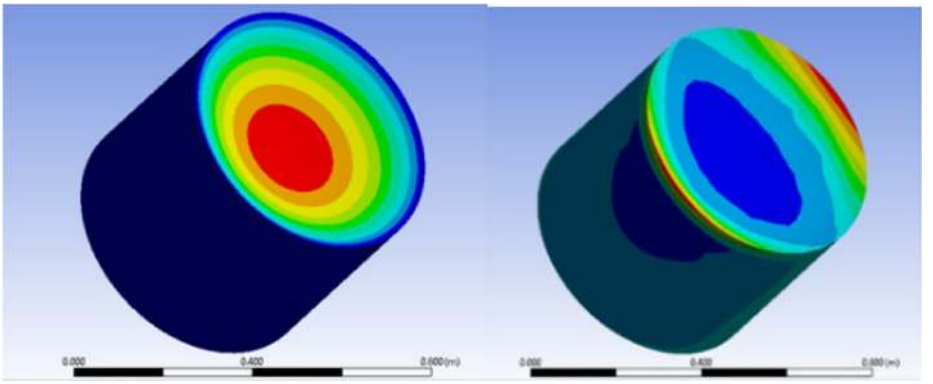

Figure 7.
ANSYS model for a flat surface under compression

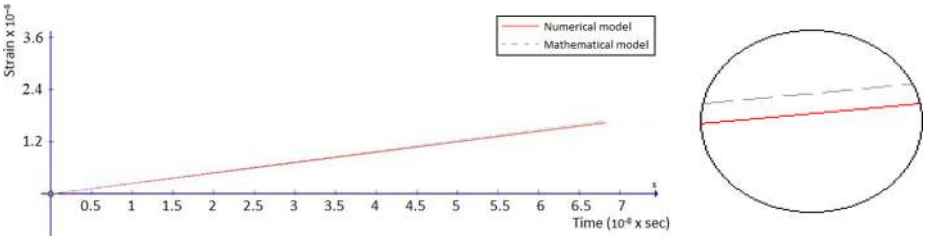

Figure 8.
Comparison of mathematical and numerical model for specific BA^{-1}

4. Case study II – turning operation

4.1 Taper turning

Consider the taper turning operation as shown in Figures 9(a)-9(b) below:

Here, the problem is usually to deal with cylindrical coordinates. Let x^m and θ are the cylindrical coordinates of the work piece before turning. After tapering, x^m will change into an inclined axis x^λ with α the angle of inclination between x^m and x^λ. Hence:

$$\frac{dx^m}{dx^\lambda} = \cos(-\alpha) = \cos(\alpha) \tag{4.1}$$

holds.

In the new, coordinate system:

$$(ds)^2 = (dx^m)^2 + R^2(d\theta)^2 \tag{4.2}$$

Therefore, metric tensor for the new coordinate system becomes:

$$g_{ij} = \begin{pmatrix} 1 & 0 \\ 0 & R^2 \end{pmatrix}$$

Table I.
Observed error in between mathematical and numerical results

Time ($\times 10^{-8}$ s)	Strain ($\times 10^{-8}$)		Error ($\times 10^{-8}$)
	Mathematical result	Numerical result	
1	0.2060	0.1999	0.0061
3	0.6151	0.5997	0.0154
5	1.0252	0.9999	0.0253
7	1.4354	1.3993	0.0361

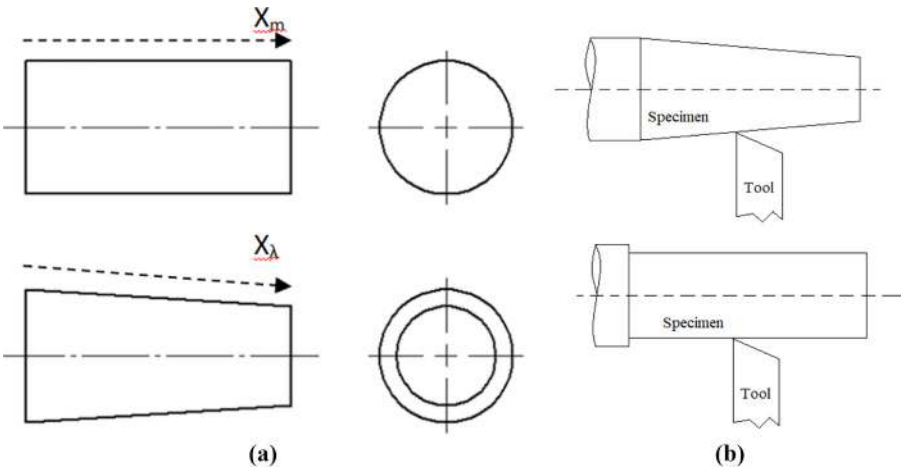

Figure 9.
(a-b): (a) represents the coordinate deployment on flat turning and tapered turning; and (b) represents the pictorial diagram of flat and taper turning operation

As we know:

$$(ds)^2 = \Sigma g_{ij} \frac{dx^i}{dy^r} \frac{dx^j}{dy^n} dy^r dy^n$$

The instantaneous metric tensor can be noticed as g_{rn}, where:

$$g_{rn} = g_{ij} \frac{dx^i}{dy^r} \frac{dx^j}{dy^n}$$

Let:

$$\frac{dx^i}{dy^r} = f_1(t), \frac{dx^j}{dy^n} = f_2(t) \tag{4.3}$$

The changing coordinates can be represented as Figure (10) shown below.

Turning strategies are the cutting procedures referring to the tool proceeds in a specific time interval. Consider Figure (10) in which, in different time intervals, t_i the slope of cutting will increase gradually and finally result in the required taper. The procedure itself is notified as one of the most familiar cutting strategies for taper cutting (as pictorially represented in Figure (10)).

We have:

$$\begin{aligned} \frac{dx^m}{dx^\lambda} &= \cos^2(\alpha) \\ \frac{dx^m}{dx^\lambda}]_t &= \cos^2(gt) \end{aligned} \tag{4.4}$$

where g is the least possible inclination angle in a taper cut, and t is the time at each stage of change in curvature. Therefore, the instantaneous metric tensor is:

$$g_{rn} = \begin{bmatrix} 1 & 0 \\ 0 & R^2 \end{bmatrix} \begin{bmatrix} \cos^2(gt) & 0 \\ 0 & 1 \end{bmatrix}$$

$$g_{rn} = \begin{bmatrix} \cos^2(gt) & 0 \\ 0 & R^2 \end{bmatrix} \tag{4.5}$$

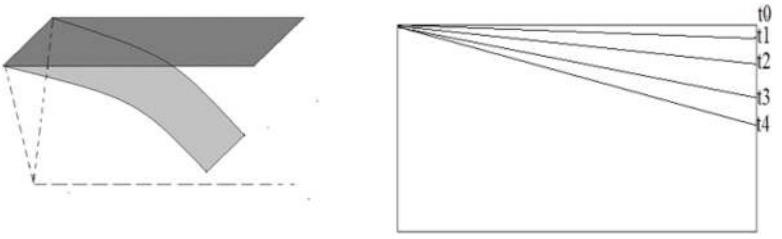

Figure 10.
Taper turning strategies

On substituting the general solution in terms of resultant tool speed and tool path:

$$\begin{bmatrix} \cos^2(gt) & 0 \\ 0 & R^2 \end{bmatrix} = A\frac{\partial}{\partial t}\left[x_y^p + x_x^p\right] + B\left[x_y^p + x_x^p\right] + \phi$$

$$\begin{bmatrix} \cos^2(gt) & 0 \\ 0 & R^2 \end{bmatrix} = A\frac{\partial}{\partial t}[\cos\Phi + \sin\Phi]x^p + B[\cos\Phi + \sin\Phi]x^p + \phi$$

$$\begin{bmatrix} \cos^2(gt) & 0 \\ 0 & R^2 \end{bmatrix} = \begin{bmatrix} a_{11} \\ a_{21} \end{bmatrix}[\cos\Phi + \sin\Phi]\frac{\partial}{\partial t}x^p + \begin{bmatrix} b_{11} \\ b_{21} \end{bmatrix}[\cos\Phi + \sin\Phi]x^p + \begin{bmatrix} \phi_{11} & \phi_{12} \\ \phi_{21} & \phi_{22} \end{bmatrix} \tag{4.6}$$

where Φ is the tool inclination angle, and R is the radius of the cylindrical specimen. ϕ represents a constant matrix.

Dynamic equation:

$$\cos^2(gt) = a_{11}\cos\Phi\frac{\partial}{\partial t}x^p + b_{11}\cos\Phi x^p + \phi_{11} \tag{4.7}$$

Static equations:

$$a_{11}\sin\Phi\frac{\partial x^p}{\partial t} + b_{11}\sin\Phi.x^p + \phi_{12} = 0,\ a_{21}\cos\Phi\frac{\partial x^p}{\partial t} + b_{21}\cos\Phi.x^p + \phi_{21} = 0,$$

and: $a_{21}\sin\Phi\frac{\partial x^p}{\partial t} + b_{21}\sin\Phi.x^p + \phi_{22} = r^2$

4.2 Heat generation when the BA^{-1} is a function of force

From Case (1), we obtained a result of the BA^{-1} ratio as proportional to the force applied:

Let the force be N in newton:

$$\frac{b_{11}}{a_{11}} = K\left[N_{x_x^p}i + N_{x_y^p}j\right] \tag{4.8}$$

Let μ be the frictional coefficient, then we have b/a in terms of this frictional force as:

$$\frac{b_{11}}{a_{11}} = \frac{K}{\mu}\left[F_{x_x^p}i + F_{x_y^p}j\right] \tag{4.9}$$

To obtaining heat energy H^P, we have to find the work done using the frictional force as follows:

$$\frac{b_{11}}{a_{11}} = \frac{K}{\mu x^p}\left[F_{x_x^p}i + F_{x_y^p}j\right].\left[x_x^p i + x_y^p j\right] \tag{4.10}$$

$$\frac{b_{11}}{a_{11}} = \frac{K}{\mu x^p}\left[F_{x_x^p}x_x^p + F_{x_y^p}x_y^p\right]$$

$$\frac{b_{11}}{a_{11}} = \frac{KL}{\mu x^p}H^P$$

$$\frac{b_{11}}{a_{11}} = \frac{K^1}{\mu x^p}H^P \tag{4.11}$$

Already, we have:

$$g_{ij} = A\left(\frac{dx^p}{dt}\right) + B(x^p) + \phi$$

$$g_{ij}A^{-1} = I\left(\frac{dx^p}{dt}\right) + BA^{-1}(x^p) + \phi A^{-1}$$

$$g_{ij}A^{-1} = I\left(\frac{dx^p}{dt}\right) + \frac{H^P}{\mu}[K^1]\left[\frac{1}{x^p}\right](x^p) + \phi A^{-1}$$

$$\begin{pmatrix} g_{11} & g_{12} \\ g_{21} & g_{22} \end{pmatrix}\begin{pmatrix} a_{11} & a_{12} \\ a_{21} & a_{22} \end{pmatrix}^{-1} = \begin{pmatrix} 1 & 0 \\ 0 & 1 \end{pmatrix}\left(\frac{dx^p}{dt}\right) + \frac{H^P}{\mu}\begin{bmatrix} K^1_{11} \\ K^1_{21} \end{bmatrix}\begin{bmatrix} \frac{1}{\cos\Phi} & \frac{1}{\sin\Phi} \end{bmatrix} + \begin{pmatrix} \phi_{11} & \phi_{12} \\ \phi_{21} & \phi_{22} \end{pmatrix}\begin{pmatrix} a_{11} & a_{12} \\ a_{21} & a_{22} \end{pmatrix}^{-1} \tag{4.12}$$

Thus, the general heat equation in terms of the Riemann curvature tensor becomes:

$$R^d_{ijk}A_z{}^{-1} = I\left(\frac{dx^p}{dt}\right) + \frac{H^P}{\mu}[K_z{}^1]\left[\frac{1}{x^p}\right](x^p) + \phi_z A_z{}^{-1} \tag{4.13}$$

This gives the relation between the instantaneous curvature, velocity, tool position, heat generated where $A_z{}^{-1}$, $\phi_z, K_z{}^1$ are constants.

4.3 Turning operation with constant depth of cut and force as a function of velocity

Consider a turning operation with constant depth of cut. A case study has been conducted in a turning operation as shown in Figure 11 and a general heat generation equation is modelled.

In this section, the normal turning operation with constant depth of cut throughout a specific length is analysed. The red portion in Figure 10 indicates the volume to be machined

Figure 11.
Normal turning operation

from the cylinder. The cutting time for each step should be extremely small (as in rapid cutting) because our modelling is based on instantaneous changing of curvature and assuming the cutting tool does not get tilted in between the process so that the resultant tool angle remains constant and normal to the cutting surface.

Let R be the radius of the cylinder, then the geodesic will be:

$$g_m = \begin{bmatrix} 1 & 0 \\ 0 & (R-gt)^2 \end{bmatrix}$$

$$\begin{bmatrix} 1 & 0 \\ 0 & (R-gt)^2 \end{bmatrix} = A\frac{\partial}{\partial t}\left[x_y^p + x_x^p\right] + B\left[x_y^p + x_x^p\right] + \phi$$

$$\begin{bmatrix} 1 & 0 \\ 0 & (R-gt)^2 \end{bmatrix} = A\frac{\partial}{\partial t}[\cos\Phi + \sin\Phi]x^p + B[\cos\Phi + \sin\Phi]x^p + \phi$$

$$\begin{bmatrix} 1 & 0 \\ 0 & (R-gt)^2 \end{bmatrix} = \begin{bmatrix} a_{11} \\ a_{21} \end{bmatrix}[\cos\Phi + \sin\Phi]\frac{\partial}{\partial t}x^p + \begin{bmatrix} b_{11} \\ b_{21} \end{bmatrix}[\cos\Phi + \sin\Phi]x^p + \begin{bmatrix} \phi_{11} & \phi_{12} \\ \phi_{21} & \phi_{22} \end{bmatrix} \tag{4.14}$$

The subsequent dynamic equation (time-dependent equation) from equation (4.14) is:

$$\begin{aligned} (R-gt)^2 - R^2 &= a_{21}\sin\Phi\frac{\partial}{\partial t}x^p + b_{21}\sin\Phi x^p \ldots\ldots\ldots\ldots\ldots \phi_{22} = R^2 \\ g^2t^2 - 2Rgt &= a_{21}\sin\Phi\frac{\partial}{\partial t}x^p + b_{21}\sin\Phi x^p \end{aligned} \tag{4.15}$$

The corresponding static equations are:

$$a_{11}\cos\Phi\frac{\partial}{\partial t}x^p + b_1\cos\Phi.x^p = 0$$

$$a_{11}\sin\Phi\frac{\partial}{\partial t}x^p + b_{11}\sin\Phi.x^p = 0$$

$$a_{21}\cos\Phi\frac{\partial}{\partial t}x^p + b_{21}\cos\Phi.x^p = 0$$

Applying the following boundary conditions in equation (4.15):

$$t = T, \frac{\partial}{\partial t}x^p = V, x^p = X$$

We get:

$$a_{21} = \frac{g^2T^2 - 2RgT}{V(\cos\Phi + \sin\Phi)}, b_{21} = 0 \tag{4.16}$$

On substitution of equation (4.16), equation (4.15) becomes:

$$g^2t^2 - 2Rgt = \frac{g^2T^2 - 2RgT}{V(\cos\Phi + \sin\Phi)}\sin\Phi\frac{\partial}{\partial t}x^p \tag{4.17}$$

From merchant circle shown in Figures 12(a)-(b), it is easy to understand how the velocity components are mutually correlated according to the merchant circle. The velocity along the cutting force $\left(\frac{\partial x^c}{\partial t}\right)$, velocity along the tangential force $\left(\frac{\partial x^t}{\partial t}\right)$ and the resultant velocity $\left(\frac{\partial x^p}{\partial t}\right)$ is considered here.

Therefore, $\frac{\partial x^p}{\partial t} = \frac{\partial x^c}{\partial t}/\cos(\beta - \alpha)$

On multiplying left-hand and right-hand side of equation (14.17) with cutting force (F_C) and substituting the resultant velocity $\left(\frac{\partial x^p}{\partial t}\right)$ in terms of the cutting velocity, we have:

$$(g^2t^2 - 2Rgt)F_C = \frac{g^2T^2 - 2RgT}{V(\cos\Phi + \sin\Phi)}\frac{\sin\Phi}{\cos(\beta - \alpha)}F_C\frac{\partial}{\partial t}x^c$$

$$(g^2t^2 - 2Rgt)F_C = \frac{g^2T^2 - 2RgT}{V(\cos\Phi + \sin\Phi)}\frac{\sin\Phi}{\cos(\beta - \alpha)}Q_C$$

where, the heat generation due to cutting force, $Q_c = F_c\frac{\partial}{\partial t}x^c$:

$$Q_C = \frac{F_C(g^2t^2 - 2Rgt)\,V(\cos\Phi + \sin\Phi)\cos(\beta - \alpha)}{\sin\Phi(g^2T^2 - 2RgT)} \tag{4.18}$$

where Φ, β and α are the tool inclination, friction angle, rake angle, respectively.

4.4 Another approach to find the total heat generated on the chip

On differentiating equation (4.17):

$$2g^2t - 2Rg = \frac{g^2T^2 - 2RgT}{V(\cos\Phi + \sin\Phi)}\frac{\sin\Phi}{M\sin\beta}M\frac{\partial^2}{\partial t^2}x^r$$

$$2g^2t - 2Rg = \frac{g^2T^2 - 2RgT}{V(\cos\Phi + \sin\Phi)}\frac{\sin\Phi}{M\sin\beta}F_r$$

$$2g^2t - 2Rg = \frac{g^2T^2 - 2RgT}{V(\cos\Phi + \sin\Phi)}\frac{\sin\Phi}{M\sin\beta.dx^p}F_r.dx^p$$

$$2g^2t - 2Rg = \frac{g^2T^2 - 2RgT}{V(\cos\Phi + \sin\Phi)}\frac{\sin\Phi}{M\sin\beta.dx^p}dH^p$$

where V is the velocity of the tool, and M is the mass of the carriage.

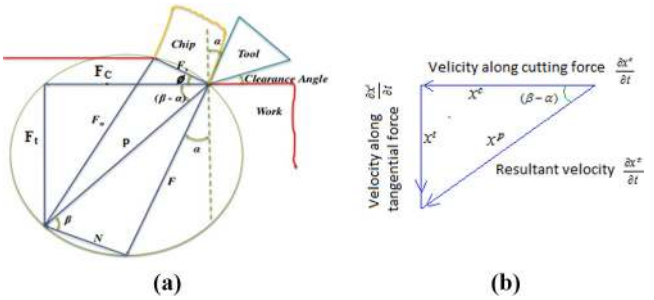

Figure 12.
(a-b) Forces acting on the tool work piece interface (a), velocity components present in the merchant circle (b)

As the tool path is helical:

$dx^{p} = \frac{2\Pi(R-gt)}{P}\,dt$ Where, P is the pitch of the helix.

Therefore, equation (4.17) becomes:

$$2g^2t - 2Rg = \frac{g^2T^2 - 2RgT}{V(\cos\Phi + \sin\Phi)} \frac{P.\sin\Phi}{M\sin\beta\,.2\Pi(R-gt)} dH^{p}$$

$$dH^{p} = \frac{(2g^2t - 2Rg)M\sin\beta\,.2\Pi(R-gt)V(\cos\Phi + \sin\Phi)}{(g^2T^2 - 2RgT)P.\sin\Phi}\,dt \tag{4.19}$$

$$H^{p} = \int_0^T \frac{(2g^2t - 2Rg)M\sin\beta\,.2\Pi(R-gt)V(\cos\Phi + \sin\Phi)}{(g^2T^2 - 2RgT)P.\sin\Phi}\,dt$$

where, H^{P} is the total heat generated.

The major portion of the heat generated is shared by the chip, and the tool in the conventional machining and the remaining share goes to the work piece and environment, respectively. However, the exact amount heat possession by each of the components may depend on many more factors; hence, in general, we can consider four components of the heat generated. These components are the heat absorbed by the tool H^{T}, the heat absorbed by the work piece $H^{w/p}$, the heat absorbed by the chip H^{C} and finally, the remaining quantity of heat energy E transmitted to the surrounding.

Therefore, $H^{P} = H^{T} + H^{w/p} + H^{C} + E$ and $1 = \Delta^{T} + \Delta^{w/p} + \Delta^{c} + e$

where: $\Delta^{T} = H^{T}/H^{P}$, $\Delta^{w/p} = H^{w/p}/H^{P}$, $\Delta^{C} = H^{C}/H^{P}$ and $e = E/H^{P}$.

The sum of these four components of the fractional heat generation (Δ) will be unitary.

5. Results

The mathematical model derived above section graphically presented and some important 2D plots and 3D surface plots arrived at. The effect of different tool angles in heat generation is studied with the help of the model equation (4.18). It is observed that the combined effect of these tool angles bears a significant role in heat generation. The effect of positive and negative rake angle is also plotted in 2D. The effect of varying cutting force for different friction angle β tracked using a 3D surface and the *locus* of the maximum heat generation is obtained using equation (4.18). The combined effect of the friction angle and the rake angle is clearly visible in terms of some mathematical trends of the heat generation as shown in Figures 13(a) and (b). It has been noticed that an increase in the negative rake angle reduces the total heat generation, as shown in Figure 13(c). The effect of cutting force is found to be linear in the heat generation equation and the associated trend related to the combined effect of the rake angle and the friction angle, as shown in Figures 14(a) and (b). An increasing negative rake angle reduces the heat generation capacity of the applied cutting force, which is visible from Figure 14(c). The heat generated by the timely varying cutting is observed using a 3D surface plot and the maximum heat generation for different ($\beta - \alpha$) studied in Figures 15(a), (b), (c). The high heat generation rate is observed at lower ($\beta - \alpha$) values. The formation of maxima in the heat generation curve in an instant of time represents the limiting point of cutting velocity after which the further heat generation declines. The mathematical modelling results are studied, and the patterns involved in between different tool angles are studied. Though the range of the rake angle generally varies from –15° to 15° and the friction angle seen is usually less than 50° in the conventional machining, the results

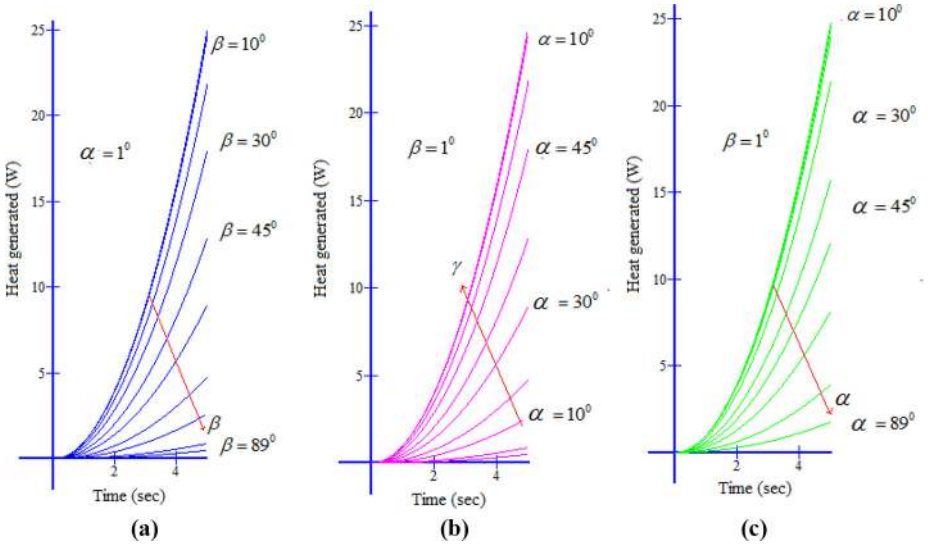

Figure 13.
(a-c) Effect of friction angle in heat generation (a), effect of positive rake angle in heat generation (b), effect of negative rake angle in heat generation (c), with solitary cutting force

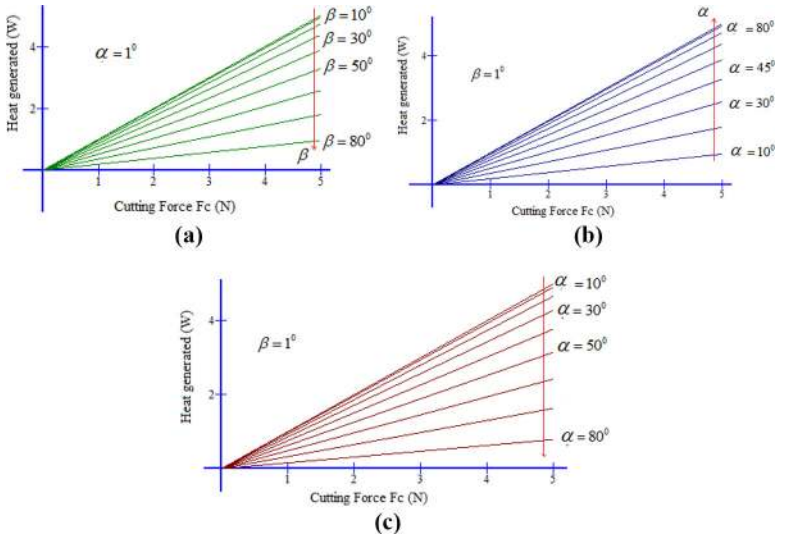

Figure 14.
(a-c) Effect of cutting force in heat generation with varying friction angle (a), Effect of cutting force in heat generation with varying (+) rake angle (b), effect of cutting force in heat generation with varying (–) rake angle (c)

incorporated here include a wide range of these angles (0° to 90°), to identify the associated mathematical patterns behind, which might be useful to understand the flexible manufacturing in an a broader perspective as the curvature effect also involved. This wide range of mathematical results also holds the required range of the rake angle and the friction angle for the conventional machining as well. This may be useful for further studies and research in the same area.

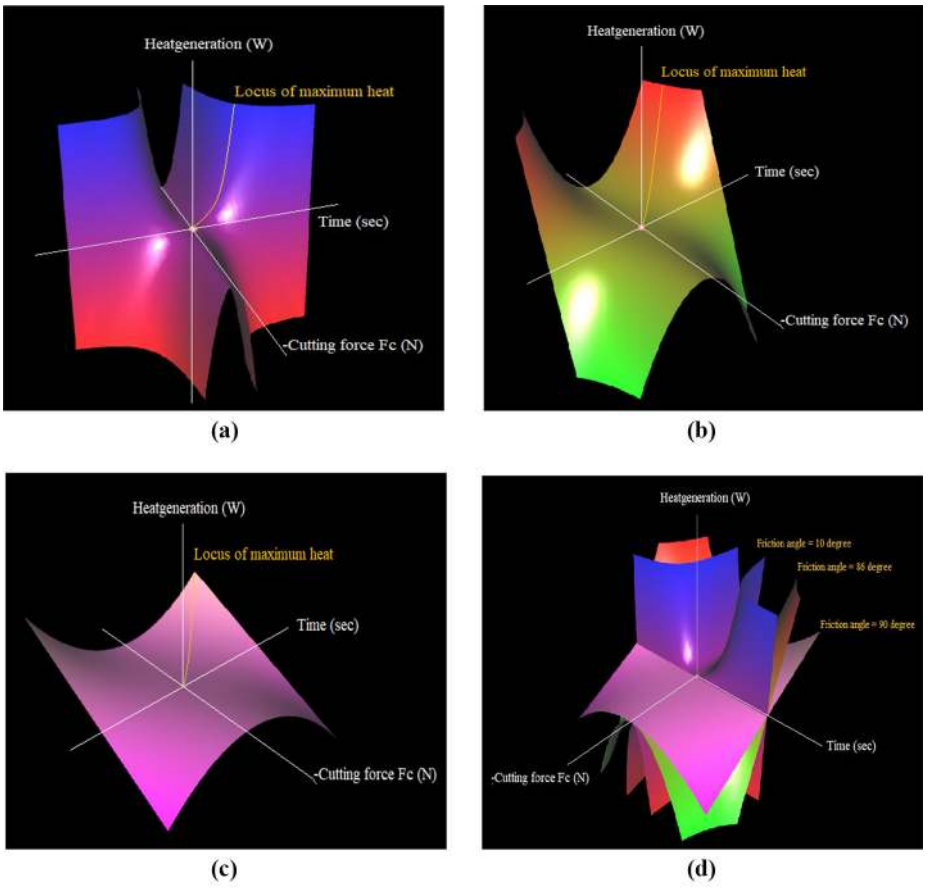

Figure 15.
(a-d) Effect of varying cutting force for friction angle $\beta = 10^{\circ}$

Notes: (a) Effect of varying cutting force for friction angle $\beta = 86^{0}$; (b) effect of varying cutting force for friction angle $\beta = 90^{0}$ (c), Combined 3D plot for (a), (b), (c)

The above graphs and explanation prove the physical symmetry of the above methodology with the existing results. Different cutting strategies for different output parameters (e.g., heat generation, stress acting on, etc.) can be compared and optimised using this mathematical methodology provided.

The use of the curvature methodology described above can be represented in tabular form as given below. Figure 16 represents the corresponding tabular model in general for the methodology discussed. Blank columns are used to represent the curvature tensor or metric tensor and correspond to the output parameter obtained from the mathematical methodology using in terms of the rate of change of curvature or relative metric tensor. Hence, the table comprises the different strategies and the effect in the required output parameter. Based on the cutting strategy, we consider the effect of the output parameters, which will differ accordingly to the strategy casted. A mathematical methodology to optimise the cutting strategy (which path should be taken to optimise certain output

parameters with respect to the rate of change in curvature while machining) has been successfully developed with different case studies, coping up with the existing true results in the field. As Table I is a random case format in general, no entries are given to describe a specific situation, as it is only meant for understanding purpose.

5.1 Validation of the methodology in terms of change in temperature

The sudden acceleration in temperature in the tool tip will be different for various materials used and have similar mathematical pattern as per the methodology described. Consider the turning operation with rake angle as zero, which correspondingly results in a situation having the rate of change of curvature zero $\left(\frac{\partial g_{ij}}{\partial t} = 0\right)$ for an instant of time t. Here, the situation is similar to the equation (3.2), where χ_i is the instantaneous temperature; χ the maximum temperature; T and t represent the total and instantaneous time, respectively; $\Delta\chi_i$ represents the change in temperature.

We know an increase in the temperature is directionally proportional to the square root of the cutting speed as provided in literatures (Carvalho *et al.*, 2006; Sun *et al.*, 2017), i.e. $\Delta\chi_i = k\left(\frac{\partial x^p}{\partial t}\right)^{0.5}$, where k represents a proportionality constant.

Therefore:

$$\frac{\partial x^p}{\partial t} = \frac{(\Delta\chi_i)^2}{k^2} \tag{5.1}$$

On further differentiation of equation (5.1) and substituting in equation (3.2), we have:

$$\begin{aligned} &\frac{2(\Delta\chi_i)}{k^2}\frac{\partial\Delta\chi_i}{\partial t} + \frac{BA^{-1}(\Delta\chi_i)^2}{k^2} = 0 \\ &\frac{\partial\Delta\chi_i}{\partial t} + \frac{BA^{-1}}{2}\Delta\chi_i = 0 \end{aligned} \tag{5.2}$$

On solving the first-order differential equation (5.2) and applying the boundary conditions $\Delta\chi_i = 0$ at $t = 0$ and $\Delta\chi_i = (\Delta\chi)_{\max}$ at $t = T$ arrives at:

$$\Delta\chi_i = e^{-0.5(BA^{-1})t} + c_1 \tag{5.3}$$

where:

$$c_1 = -1 \text{ and } BA^{-1} = -(2/T).\ln\left[(\Delta\chi)_{\max} + 1\right] \tag{5.4}$$

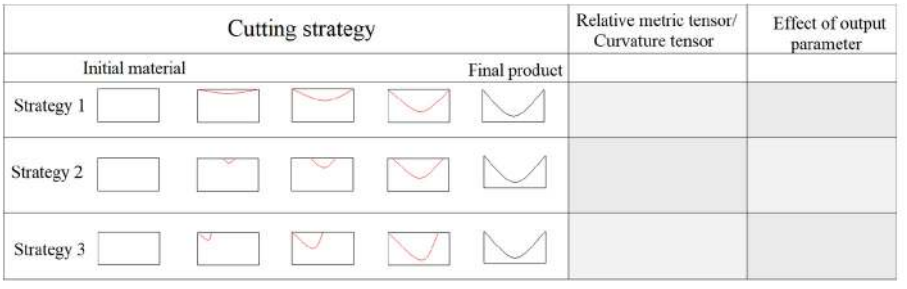

Figure 16. Format for optimisation table for different cutting strategy

From equation (5.4), it is evident that BA^{-1} is a function of the total time and the maximum change in temperature. As per our observation, the maximum temperature change is found to be depending on the material properties, and hence, for any two different materials, BA^{-1} should be different and $\Delta\chi_i$ has to follow similar patterns in accordance with equation (5.3). This can be validated by using two different materials like mild steel and titanium, by recording their temperature increase in a very short span of time, keeping all other parameters uniform throughout the experiment. The temperature is measured in the tool tip with the help of a sensitive thermocouple in a spindle speed of 710 rpm, feed rate of 0.15 mm/rev and depth of cut of 0.3 mm. The cutting tool used is cubic boron nitride (CBN). The experimental and mathematical results are obtained and plotted in Figures 17(a)-(b), where Figures 17(a) and (b) represent the timely temperature distribution of mild steel and titanium alloy (Ti-6Al-4V), respectively.

From the experiment conducted, BA^{-1} values observed for the material mild steel is –0.4796, and for titanium alloy (Ti-6Al-4V), is –0.5545. Despite the slight deviations between the mathematical and experimental results observed, on account of the assumptions taken in the methodology, sensitivity of the temperature measuring apparatus and other manual errors, the two graphical plots in Figures 17(a)-(b) are found following quite similar and close trends in the experimental results obtained and mathematical model developed. Hence, equation (5.3) should be treated as a mathematical model of best fit to describe the abovementioned situation. This yet again notified the significance of BA^{-1} and likewise, validated the mathematical methodology, in terms of the temperature build-up on the tool tip. And also, the study can be extended for the optimisation of the cutting strategy (rate of change in curvature chosen) by controlling the input parameters, to reduce the acceleration of temperature built up, in a curvature perspective.

6. Conclusions

A mathematical modelling and procedure has been developed and can be applied to study the effect of mechanical properties in terms of instantaneous curvatures and thereby optimising the cutting strategy accordingly in the case of certain parameters associated. The study will find application in a highly flexible subtractive manufacturing operation and is expected to be one of the basic models for the cutting strategy optimization in flexible and simultaneously multi-dimensional cutting operations in the rate in curvature perspective. Case studies are conducted under uniform compression forging and turning operation and

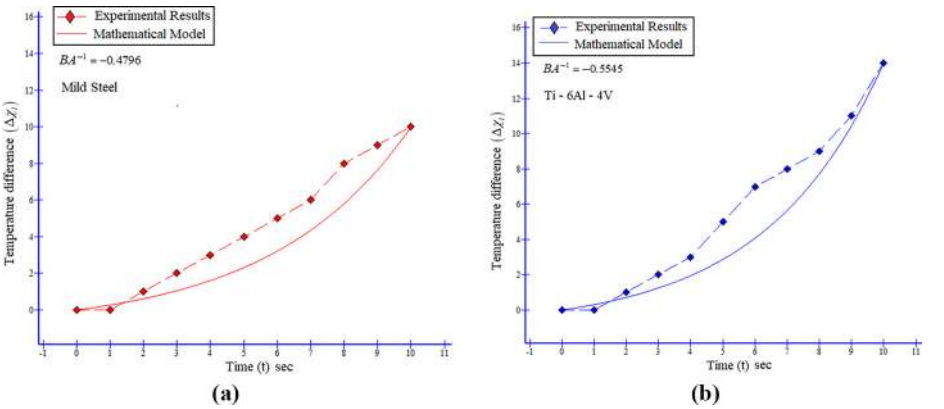

Figure 17.
(a-b) Time-based temperature difference plot for mild steel material (a), time-based temperature difference plot for Ti-6Al-4 V alloy (b)

are applied to find heat generation in a turning operation and also validate (in terms of temperature rise) the model with existing results. The same model is applied to track the trends of the different cutting angles like the friction angle, rake angle and cutting force. It is expected that the extension of this methodology, through analysing BA^{-1} ratio in the field of forging and casting processes, where the instantaneous curvature affects the different mechanical properties significantly, will find more practical applications in the near future.

The results obtained in the different case studies and their profound use to understand the contribution of different tool angles in the undesirable outputs like heat generation in a turning operation, where the rate of change of curvature plays an important role, should be considered. The curvature focused study in the forging operation likewise paved the path to identify the behaviour of internal strain in a uniform compression process and in more general situation where the rate of curvature having some valid metric tensor. The current limitation of the conventional machining is the solo-strategic cutting mechanism involved in many machining process; still, there are flexible machining operations that can be observed in some cases and the importance of this multi-strategic machining is getting increased in parallel terms. The mathematical methodology introduced here anticipates the identification of the optimal cutting strategy that has to be pursued to reduce certain unwanted outputs like heat generation and internal strain.

The impact of the rake angle and friction angle on the total heat generated is studied in terms of the mathematical model obtained from the methodology developed. It has been observed that an increment within the negative rake angle diminishes the overall heat generation. The effect of cutting force is found to be in direct proportion with the heat generated. An expanding negative rake angle decreases the heat generation in accordance with the cutting force for the specific cutting strategy used in the case study. The result and impact of the tool angle in the heat generation are found fundamentally correlated with the curvature strategy taken. It is also identified that the distribution of maximum heat generation in a small tenure reaches to a point of constraint based on the cutting speed applied, after which the advancement of further heat generation decays for the specific curvature-based strategy. Finally, a strategy created is validated in terms of temperature rise in tool tip for encouraging clarity. The work enables to identify the importance of the curvature difference and rate of change of curvature in a modern manufacturing scenario, as the emerging technologies like 3D printing and 4D printing using shape memory polymers demand more curvature and shape-based methodologies and modelling in the field.

References

Abhang, L.B. and Hameedullah, M. (2010), "Chip-tool interface temperature prediction model for turning process", *International Journal of Engineering Science and Technology*, Vol. 2 No. 4, pp. 382-393.

Abukhshim, N.A., Mativenga, P.T. and Sheikh, M.A. (2006), "Heat generation and temperature prediction in metal cutting: a review and implications for high speed machining", *International Journal of Machine Tools and Manufacture*, Vol. 46 Nos 7/8, pp. 782-800.

Attia, M.H., Joseph, P.M. and M'Saoubi, R. (2016), "Determination of convective heat transfer from rotating workpieces in dry and laser-assisted turning processes", *Advances in Materials and Processing Technologies*, Vol. 2 No. 2, pp. 324-338.

Ay, H. and Yang, W.J. (1998), "Heat transfer and life of metal cutting tools in turning", *International Journal of Heat and Mass Transfer*, Vol. 41 No. 3, pp. 613-623.

Borisenko, A.I. and Tarapov, I.E. (1979), *Vector and Tensor Analysis with Applications*, Dover Publications, New York, NY.

Carvalho, S.R., e Silva, S.L., Machado, A.R. and Guimaraes, G. (2006), "Temperature determination at the chip–tool interface using an inverse thermal model considering the tool and tool holder", *Journal of Materials Processing Technology*, Vol. 179 Nos 1/3, pp. 97-104.

Denkena, B., Brüning, J., Niederwestberg, D. and Grabowski, R. (2016), "Influence of machining parameters on heat generation during milling of aluminum alloys", *Procedia Cirp*, Vol. 46, pp. 39-42.

Dodson, C.T.J. and Poston, T. (2013), *Tensor Geometry: The Geometric Viewpoint and Its Uses, Vol. 130*, Springer Science and Business Media.

Fata, A., Bagheri, M. and Mottaghizadeh, P. (2012), "Tool temperature prediction during machining by FEM with experimental validation", *Journal of Basic and Applied Scientific Research*, Vol. 2 No. 12, pp. 12606-12610.

Klocke, F., Brockmann, M., Gierlings, S. and Veselovac, D. (2015), "Analytical model of temperature distribution in metal cutting based on potential theory", *Mechanical Sciences*, Vol. 6 No. 2, pp. 89-94.

Kumar, M.P., Amarnath, K. and Kumar, M.S. (2015), "A review on heat generation in metal cutting", *International Journal of Engineering and Management Research (Research)*, Vol. 5 No. 4, pp. 193-197.

Lazoglu, I. and Altintas, Y. (2002), "Prediction of tool and chip temperature in continuous and interrupted machining", *International Journal of Machine Tools and Manufacture*, Vol. 42 No. 9, pp. 1011-1022.

Li, K.M. and Liang, S.Y. (2006), "Modeling of cutting temperature in near dry machining", *Journal of Manufacturing Science and Engineering*, Vol. 128 No. 2, pp. 416-424.

McIntosh, C.B.G. and Halford, W.D. (1981), "Determination of the metric tensor from components of the Riemann tensor", *Journal of Physics A: Mathematical and General*, Vol. 14 No. 9, p. 2331.

Melzi, N., Temmar, M. and Ouali, M. (2017), "Applying a numerical model to obtain the temperature distribution while machining", *Acta Physica Polonica A*, Vol. 131 No. 3, pp. 504-506.

Narain, R., Pfaff, T. and O'Brien, J.F. (2013), "Folding and crumpling adaptive sheets", *ACM Transactions on Graphics (Graphics)*, Vol. 32 No. 4, p. 51.

O'Neill, B. (2006), *Elementary Differential Geometry*, Elsevier.

Onyechi, P.C., Oluwadare, B.S. and Obuka, N.S.P. (2013), "Analytical modeling of temperature distribution in metal cutting: finite element approach", *International Journal of Engineering Science*, Vol. 2 No. 4, p. 17.

Ostafiev, V., Kharkevich, A., Weinert, K. and Ostafiev, S. (1999), "Tool heat transfer in orthogonal metal cutting", *Journal of Manufacturing Science and Engineering*, Vol. 121 No. 4, pp. 541-549.

Patru, E.N., Bica, M., Panduru, D. and Craciunoiu, N. (2019), "Experimental studies regarding the influence of cutting parameters on tool temperature in milling process of aluminum alloys", *Advanced Engineering Forum*, Vol. 34, pp. 34-39.

Pervaiz, S., Deiab, I., Wahba, E.M., Rashid, A. and Nicolescu, M. (2014), "A coupled FE and CFD approach to predict the cutting tool temperature profile in machining", *Procedia CIRP*, Vol. 17, pp. 750-754.

Putz, M., Schmidt, G., Semmler, U., Oppermann, C., Bräunig, M. and Karagüzel, U. (2016), "Modeling of heat fluxes during machining and their effects on thermal deformation of the cutting tool", *Procedia Cirp*, Vol. 46, pp. 611-614.

Ribeiro, S., Fernandes, A.P., Cunha, D.F.D., Silva, M.B.D., Shan, J. and Guimaraes, G. (2018), "Estimation of a moving heat source due to a micromilling process using the modified TFBGF technique", *Mathematical Problems in Engineering*, Vol. 2018.

Subbiah, S. and Melkote, S.N. (2008), March). "On the size-effect in micro-cutting at low and high rake angles", *ASME 2004 International Mechanical Engineering Congress and Exposition*, American Society of Mechanical Engineers Digital Collection, pp. 485-493.

Sun, Y., Sun, J. and Li, J. (2017), "Modeling and experimental study of temperature distributions in end milling Ti6Al4V with solid carbide tool", Proceedings of the Institution of Mechanical Engineers, Part B: Journal of Engineering Manufacture, *231*(2), 217-227.

Uzorh Augustine, C. and Nwufo Olisaemeka, C. (2013), "Thermal aspects of machining: Evaluation of tool and chip temperature during machining process using numerical method", *The International Journal of Engineering and Science*, Vol. 2 No. 4, pp. 66-79.

Corresponding author
Rajyalakshmi G. can be contacted at: rajyalakshmimed@gmail.com